Harnessing native iron ore as an efficient electrocatalyst for overall water splitting

Md Abu Sayeed, Graeme J. Millar and Anthony P. O'Mullane*

Abstract: Electrochemical water splitting is a widely accepted approach to generate hydrogen at a scale that is suitable for storing renewable energy. Therefore the choice of catalyst for the hydrogen evolution reaction (HER) and oxygen evolution reaction (OER) are critical in terms of cost when scaling up this technology. Therefore earth abundant transition metals oxides and sulphides have received significant attention as catalysts for the OER and HER respectively. However very few examples of actual Earth abundant materials mined from the Earth's crust have been used as electrocatalysts for these reactions. Here, we demonstrate that a raw iron ore is active for both the HER and OER under alkaline conditions which is due to the natural abundance of the key elements of iron, nickel and sulphur. The catalyst is stable for both reactions and can operate at 100 mA cm^{-2} which is comparable to many chemically synthesised nanomaterials based on these elements. This approach may be attractive for adding value to iron ore while minimising the cost of catalyst production.

Introduction

Electrochemical water splitting as a means to create green hydrogen has received significant attention due to the rapid deployment and reduction in cost of renewable energy sources such as wind and solar. Recently it has been reported that this concept is economically viable for applications that are compatible with small and medium scale hydrogen supply with the projection that industrial scale supply will occur within a decade.[1] However, to ensure that this situation will occur, the continuous development of electrolyser technology is required. In particular, further development of electrocatalysts that are employed for the hydrogen evolution reaction (HER) and oxygen evolution reaction (OER) is necessary. A significant effort is being undertaken to replace expensive materials that are currently used for these reactions such as Pt, RuO_2 and IrO_2.[2] A variety of low cost transition metal phosphides, selenides, sulphides and nitrides of predominantly cobalt, nickel and iron have shown good performance for the HER [3-5] as well as their oxides for the OER,[6-12] and even stainless steel. Other examples include oxides of manganese for the OER[13-14] and sulphides and phosphides of molybdenum for the HER.[15-19] Greater detail can be gained by inspection of recent reviews on this topic.[20-23]

A critical challenge is the synthesis of electrocatalysts that are active for both the HER and the OER as this would simplify the manufacturing process for electrolysers. Several of the previously mentioned materials have been investigated for both reactions. However, a complicating factor is the generally accepted insight that the metal oxide/oxyhydroxide active forms of metal phosphides, sulphides and selenides are only formed during the OER.[24-25] Therefore the design of any bifunctional electrocatalyst needs to take this fact into consideration. This complication is of particular importance for alkaline electrolysers that are prone to reverse current flow during shut down or rapid turn down which results in oxidation of the cathode and reduction of the anode.[26] As a result, direct integration of these electrolysers with an intermittent energy source is demanding.

In terms of new electrocatalyst development recent reports have demonstrated that chemical synthesis is not always required for the discovery of active materials for electrochemical water splitting. Nature has provided minerals with many of the active species required for water splitting such as Fe, Ni and S. In particular the combination of Fe and Ni is highly effective for the OER, whereas sulphides of these metals are active HER electrocatalysts. Recently Pentlandite rocks which contain these elements showed activity for the HER under acidic conditions.[27] It has also been reported that a Gibeon meteorite was active for the OER; however, electrochemical restructuring for many hours was required to enrich the surface with oxides of Co–Ni–Fe.[28] Recently it was discovered that an iron ore when covered by a thin layer of NiOOH showed good OER activity under alkaline conditions which again took advantage of the synergy between Fe and Ni for this reaction.[29] However, there has not been any report that has demonstrated that a naturally occurring material is active for both sides of the water splitting reaction. Therefore, it would be preferable if a naturally occurring mineral could be used directly for overall water electrolysis with minimal processing or surface modification. The benefits would be twofold: (1) value adding of the resource suitable for cost effective production of water splitting catalysts; (2) new insights into the fundamental chemistry of catalysts prepared from ore bodies.

Therefore, from these initial scarce but useful studies it is postulated that careful selection of ore samples comprising of catalytically active elements may result in discovery of new, economical, and highly active electrocatalysts for electrochemical water splitting. In this study iron ore deposits were examined which comprised of the essential elements required for HER and OER activity; namely Fe, Ni and S. Iron ores from different geological sites were investigated and a particular ore containing pyrrhotite and pentlandite species within the rock composition was of particular interest. Significantly, pyrrhotite is a major source of sulphur and pentlandite contains both Ni and Fe. It was shown that this material was indeed active for the HER in its pristine state and was also active for the OER under alkaline conditions. The identification of naturally occurring deposits may be a contributing step forward for the sustainable development of green hydrogen production.

School of Chemistry, Physics and Mechanical Engineering, Queensland University of Technology (QUT), Brisbane, QLD 4001, Australia
E-mail: anthony.omullane@qut.edu.au

Supporting information for this article is given via a link at the end of the document.

Results and Discussion

The as-received raw ore was characterised by X-ray diffraction (XRD) (Figure S1). The data indicated the presence of highly crystalline species such as pyrrhotite ($Fe_{1-x}S$ (x = 0 to 0.2),

sepiolite ($Mg_4Si_6O_{15}(OH)_2 \cdot 6H_2O$), clinochlore ($Mg_{3.75}Fe_{1.25}Si_3Al_2O_{10}(OH)_8$) and pentlandite ($(Fe,Ni)_9S_8$). To investigate the electrocatalytic properties of the sample it was mixed with Nafion® to prepare a catalyst ink (details in the experimental section) which was deposited onto a glassy carbon substrate to form a uniform catalyst film. This was chosen as an approach to mimic the fabrication of an ion exchange membrane assembly. The as-deposited film was then cycled from -0.6 to 1.6 V vs RHE to investigate its suitability for the OER and from 0.3 to -0.6 V to study the HER. The optimised mass loading of the catalyst onto the glassy carbon electrode was initially investigated for the best OER performance (Figure 1a). As with many metal oxide catalysts the performance improved with potential cycling.[12] Notably however, only 5 cycles were required to activate the catalyst for the best OER performance (Figure S2) which is significantly less when compared to a previous study on a Gibeon meteorite that required 20 h of ageing for optimal performance.[28] Therefore all the data shown in Figure 1a was for the 5th potential cycle. The data indicated that an optimum level of loading was 6 mg cm^{-2} (Sample S2) and any increase in loading resulted in reduced current density for the OER. For sample S2 the overpotential at a current density of 10 mA cm^{-2} was 270 mV with a low Tafel slope value of 67 mV dec^{-1}. The data for other catalyst loadings is summarised in Table 1. This result was comparable to a previous study of an iron ore catalyst; however, a critical difference in that study was that modification with a surface layer of NiOOH was required to induce OER activity.[29] Therefore, the inherent activity of the pristine iron ore in this study was promising and presumably originated from the presence of the Ni containing pentlandite phase as discussed later. Typically for a catalyst containing Ni species there is an observable oxidation process prior to the onset of the OER (which forms the active state of the electrocatalyst). Figure 1b shows that this redox process was also present on this sample as evidenced by the broad redox feature at 1.45 V, which was prevalent for the samples with lower loading (S1-S3). The magnitude of the overall current in the zoomed in region was directly related to the mass loading of the sample; however, the increase in current seen in this range did not translate into improved OER performance. Indeed, the performance decreased once a loading of 6 mg cm^{-2} was exceeded (Table 1). This result indicated that increasing the amount of sample did not increase the number of available active sites for the OER and may be related to a decrease in electrical conductivity of the sample as expected for iron ore. Correspondingly, the redox process observed for the lower loading of samples was totally obscured at higher loadings. It is known that undoped Fe oxide based catalysts are generally poor materials for the OER,[4d] however in this case even at low concentration the additional presence of Ni in the raw ore facilitated good OER performance. The current density was consistent with previous Fe-Ni systems; albeit, Fe rather than Ni was the dopant.[6, 30-32]

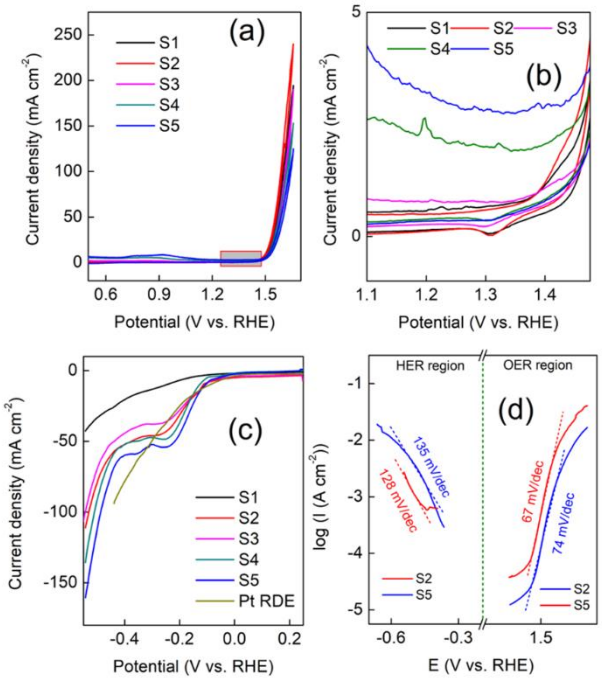

Figure 1. Electrochemical characterization of the raw ore: a) OER polarization curves recorded at 50 mV s^{-1}, b) enlarged region of the polarization curve indicated in a), c) HER polarization curves recorded at 5 mV s^{-1} and d) Tafel value both in OER and HER region.

Table 1. Different mass loading and their electrochemical performance.

Sample	Mass loading (mg cm^{-2})	Tafel slope (OER) mV dec^{-1}	OER Overpotential (mV) at 10 mA cm^{-2}	Tafel slope (HER) mV dec^{-1}
S1	3	70	280	162
S2	6	67	270	148
S3	9	70	290	145
S4	12	72	292	135
S5	15	74	297	128

The catalyst was also stable for the OER at a constant current of 10 mA cm^{-2} and the potential did not vary significantly over a period of 24 h (Figure S2b). There have been several reports relating to metal sulphide catalysts which demonstrated that the surface was in fact oxidised into metal oxide/oxyhydroxide species which were concluded to be the active form of the catalyst for the OER (accompanied by a reduction in the surface concentration of sulfur).[18, 24-25] However, it has been postulated that the formation of –OOH intermediates from the coordinated OH groups on the surface of the catalyst can be encouraged by the delocalized electrons among the attached oxygen, metal centre, and the electronegative S atoms. Therefore the formation of repulsive 3p–2p sites (3p orbital of these heteroatoms and 2p orbital of oxygen) accelerates the oxidation of the –OOH intermediate and finally promotes OER activity.[18]

Given that this ore contained metal sulphides such as pyrrhotite and pentlandite in the pristine state; in principle it should also demonstrate activity for the HER. Although it is emphasised

that under alkaline conditions this reaction is more challenging when compared to acidic conditions.[18] Nevertheless, both nickel and iron sulphide catalysts have been identified as suitable materials for the HER under strongly alkaline conditions.[33-34] Illustrated in Figure 1c are linear sweep voltammograms recorded for samples S1-S5. A distinct cathodic process was seen with a peak at ca. -0.25 V followed by a larger increase in current until the end of the sweep which was due to the HER. The redox process prior to the onset of the HER can be attributed to the Fe(III) to Fe(II) process for a FeS_2 material.[35] As for the case of the redox process prior to the OER (Figure 1b) the response increased with sample loading. However the magnitude of the HER did not increase significantly as more clearly seen when the data was normalised to the magnitude of the cathodic redox process (Figure S3). With this observation in mind Sample S2 can also be taken as an effective HER catalyst to minimise the amount of catalyst required for the reaction as the Tafel slope value of 148 mV dec^{-1} was comparable to Sample S5 with a value of 128 mV dec^{-1} (Figure 1d). The long term stability of the catalyst was tested under a constant current density of -10 mA cm^{-2} where no deviation in the applied potential was observed (Figure S2b). To further probe the effect of catalyst loading on the HER and OER, electrical impedance spectroscopy (EIS) experiments were undertaken in the OER and HER potential regions (Figure 2a-d). Experiments were undertaken under both potentiostatic (Figures 2a and c) and galvanostatic (Figures 2b and d) conditions. Under the latter conditions the catalysts should be turning over at the same rate and this data indicates that sample S2 shows lower resistance to charge transfer compared to Sample S5, in particular for the HER. This can be attributed to the increased electrical resistance for the higher loaded sample (Sample S5) due to the low conductivity of materials of this type. Therefore, Sample S2 was the optimal loading that can be used for both the HER and the OER; and was therefore investigated further for overall water splitting performance. As noted previously, for the ease of preparation of electrodes for use in an electrolyser, if the same catalyst can be used for the anode and the cathode then that is advantageous. Overall electrochemical water splitting was undertaken at an increased current density of 100 mA cm^{-2} to test the robustness of the electrodes under more demanding conditions (Figure 2c). To maintain this current density the cathode required an applied potential of ca. -0.70 V and the anode required ca. 1.7 V to give an overall cell voltage of 2.4 V which remained stable over a 3 h period. The dual action performance for both HER and OER of this catalyst was comparable with previous studies of iron, nickel and sulphur based catalysts.[36-38] However, it was found that the cathode should not be subjected to the OER prior to the HER as this strategy resulted in significant degradation of the cathode material (Figure S4). This is an issue in commercial electrolysers operated under rapid shut down and start up conditions, where reverse current can flow and thus oxidise the cathode.[26] It must be considered that for implementation into a commercial system, ideally catalysts should be grown on the electrodes themselves such as Ni foam or stainless steel, however these results indicate that natural materials show interesting properties and indeed face the same challenge of stable adherence to electrodes as their synthetically prepared counterparts. Perhaps fabricating membrane electrode assemblies for utilisation in the next generation of anion exchange membrane electrolysers[39-40] is the most appropriate way forward for this type of material. To understand the origin of the activity of this material a detailed structural and chemical analysis was undertaken.

The grazing incident XRD patterns of the as-deposited and activated catalyst after 5 potential cycles into the OER region are compared in Figure S5. The majority of the peaks remained in the same position. However, some of the peaks were intensified such as those at 2θ = 35.5° and 36.5° which corresponded to the pyrrhotite and pentlandite materials.[27, 41] Therefore, the potential cycling process was influencing the crystallinity of the material which subsequently resulted in a 3 fold improvement in the current density of the catalyst for the OER at 1.7 V (Figure S2).

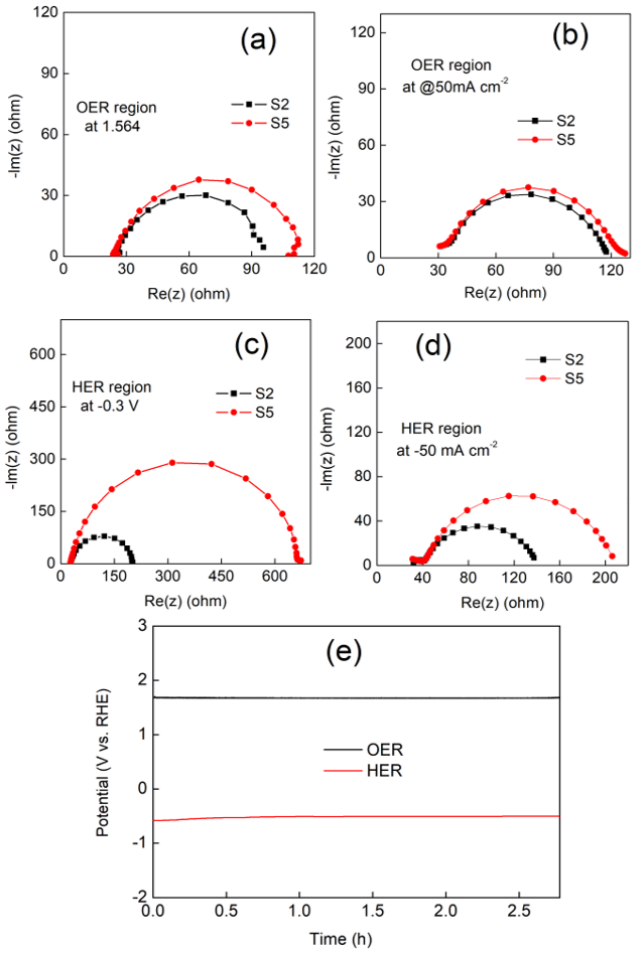

Figure 2. Nyquist plot for Samples S2 ad S5 in the OER region under constant potential (a) and galvanostatic conditions (b) and in the HER region under constant potential (c) and galvanostatic conditions (d); stability test for Sample S2 under a constant current of 100 mA cm^{-2} for the OER and HER.

Figure 3 shows the high-resolution transmission electron microscope (HR-TEM) characterisation of the raw (Figure 3a and b) and the activated (Figure 3c and d) material. The as received ore was observed with a consistent lattice spacing of 0.29 nm throughout the sampled region (Figure 3b) which corresponded to the pyrrhotite (300) superstructure which was the major constituent of the ore[42] and close to the spacing of 0.297 nm seen for the hexagonal structure of pure Fe_7S_8.[36] The selected area diffraction (SAED) pattern (inset of Figure 3a) showed evidence of rings in the pattern (indexed to the (300) and (110) planes of Fe_7S_8) that contained several individual reflections corresponding to different orientations of the crystals (which was not unexpected for a natural ore sample). Interestingly, after potential cycling in the OER region (Figure 3c) the TEM image (Figure 3c) shows that the material became slightly more porous and the HRTEM image (Figure 3c) revealed clear lattice fringe spacings of 0.245 nm,

0.276 nm and 0.30 nm; which can be indexed to the (202), (113) and (300) planes of Ni_3S_2 (Fe-Ni_3S_2).[38] Also, the ring pattern became more pronounced and indexed to the (202), (113) and (300) planes of Ni_3S_2. In addition, the number of spots within each ring increased which again suggested the presence of a significant number of crystals with different orientations. Therefore electrochemical activation resulted in a change in the morphology, crystallinity and composition of the material which was beneficial for the OER (Figure 1a) but inhibited the HER (Figure S4).

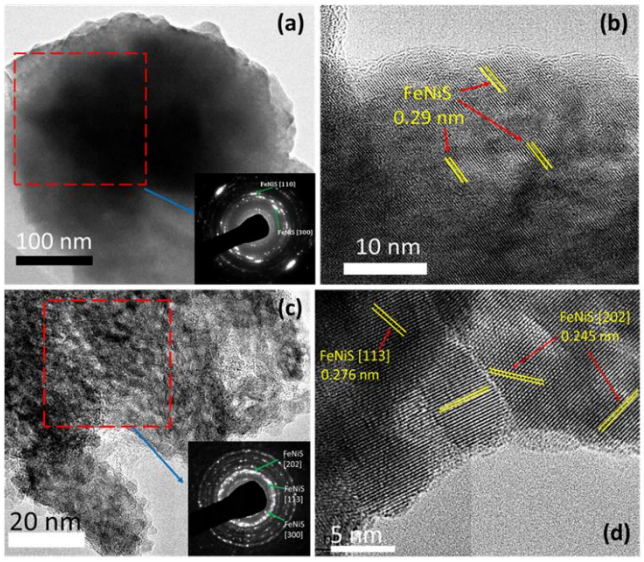

Figure 3. HR-TEM images of raw material (a-b) and activated within the water splitting region (c-d).

To further probe the changes that occurred upon potential cycling, scanning TEM dark field (STEM-DF) imaging combined with energy dispersive X-ray spectroscopy (EDX) was undertaken. A uniform distribution of Fe, S, and Ni was observed in the raw material (Figure 4a). The composition was analysed by EDX and as expected was dominated by the presence of Fe, S and O with a notably lower concentration of Ni. However, upon electrochemical potential cycling the morphology changed as well as the distribution of the elements within the material. In particular, a significant reduction in the intensity of the S component was recorded. It was also seen that in certain areas the Fe, Ni, and S elements accumulated to form an iron nickel sulphide material as suggested by the HRTEM imaging (Figure 3d). In addition, the oxygen content increased which was expected as a result of the material being electrochemically oxidised. This study indicated that sulphur is removed from the catalyst material due to this oxidation process and was most likely the reason for the reduced HER performance after potential cycling. This conclusion was also consistent with previous work on electrochemically formed NiS_x materials.[25] This loss of sulphur was also seen with elemental mapping using SEM-EDX on a larger scale (Figure S6) and therefore this phenomenon was prevalent across the entire sample. Evidence of sulphide oxidation was also inferred from cyclic voltametric data (Figure S7) which showed a broad oxidation process at 0.90 V that increased with catalyst loading. This behaviour was again consistent with the electrochemical oxidation of sulphide under alkaline conditions into polysulfide S_2^{2-} species.[43]

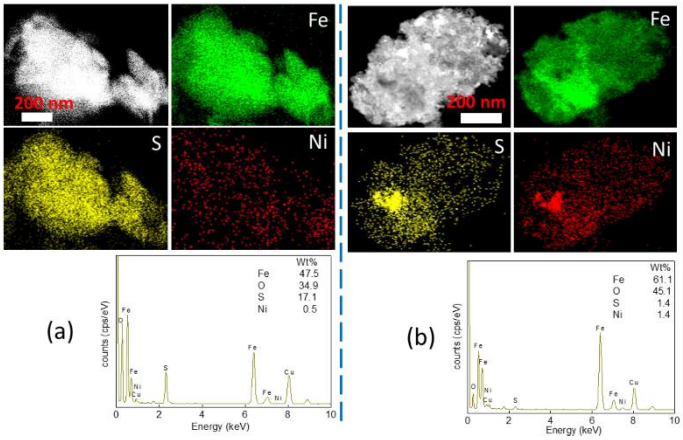

Figure 4. STEM-DF images and the corresponding EDX maps and elemental composition of (a) raw ore and (b) after electrochemical conditioning showing the Fe, S, and Ni in the iron ore catalyst.

Electrochemical reactions are dominated by the surface of an electrode. Therefore to probe the composition of the catalyst as well as the oxidation states of the elements at the surface, XPS was undertaken of the pristine and activated iron ore. Figure 5a shows the XPS spectrum of the Fe 2p core level. The peaks for the raw ore (Upper panel, Figure 5a) from 708 to 717 eV were for Fe $2p_{3/2}$ and indicated the presence of Fe^{2+} and Fe^{3+} oxidation states with a satellite peak at 720.1 eV.[36] Whereas the peak at 724.8 eV was characteristic of the oxidation state of a nickel iron sulphide composite.[44] This observation was also consistent with previous work on ultrathin Pyrrhotite Fe_7S_8 nanosheets.[36] After electrochemical activation (lower panel, Figure 5a), there were slight shifts in the position of the Fe $2p_{1/2}$ peaks which when deconvoluted indicated the presence of a ternary nickel-iron sulphide catalyst.[37] The Ni $2p_{3/2}$ XPS spectrum of the raw ore showed peaks at 853.2 and 856.3 eV and a satellite peak at 861.7 eV (Upper panel, Figure 5b) which corresponded to Ni $2p_{3/2}$ which was characteristic of the Ni^{2+} oxidation state and was consistent with previous work on iron nickel sulphide nanosheets[38] and pyrrhotite and pentlandite.

Interestingly, similar to a previous study on iron ore, after electrochemical activation there was a minor peak at 858.3 eV which was the characteristic of NiOOH formation (lower panel, Figure 5b)[29] which is known to be a highly active form for the OER. The O 1s XPS spectra for the raw ore and activated ore are shown in Figure 5c. The observed peaks at 530.9 and 532.3 eV (upper panel, Figure 5c) were due to metal hydroxide (M-OH) bonds and O^{2-} incorporation in the subsurface of the film, respectively; which is common in transition metal oxides.[45] After electrochemical activation a strong peak emerged at 529.7 eV, indicating a nickel ferrite lattice oxygen[45] while the peak due to O^{2-} incorporation in the subsurface of the film decreased in intensity; however, the peak due to M-OH persisted. For the S 2p spectrum there was a broad feature with two peaks at 168 and 171 eV eV (Figure 5d) which was attributed to oxidised sulphur species such as sulfate and sulphite, respectively;[44, 46-47] which was not surprising for a natural iron ore sample. After activation, the intensity of the S 2p peaks was reduced (lower panel, Figure 5d), indicating a decrease in surface concentration which was consistent with the HRTEM and SEM data described above. After the activation process, the sulphite peak disappeared and was

presumably oxidised to sulfate as these peaks persisted; albeit, at a significantly reduced intensity compared to the pristine iron ore. However, two new peaks emerged at 162.9 and 164.3 eV which were attributed to S^{2-} and S_2^{2-} species, respectively.[48]. Again, the data was consistent with the presence of iron-nickel sulphide on the surface of the material.

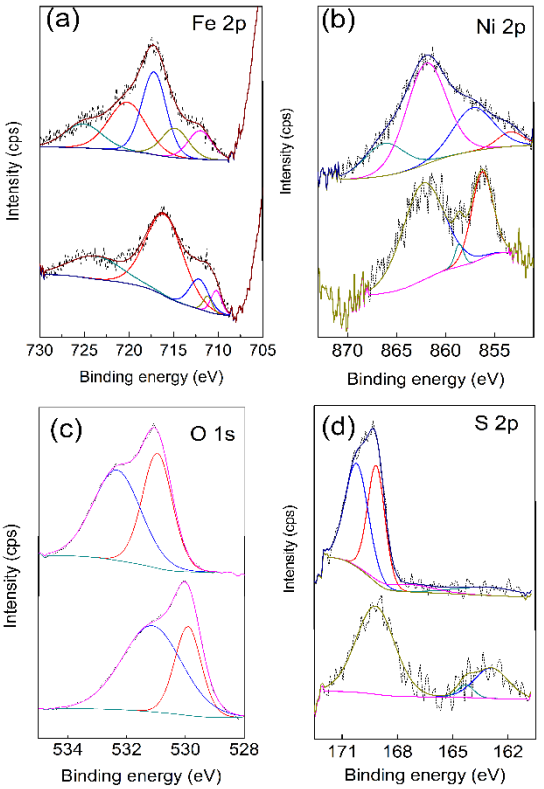

Figure 5. XPS surface analysis for as-deposited (upper panel) and activated $FeNiS_2$ catalysts (lower panel) a) Fe 2p, b) Ni 2p, c) O 1s and d) S 2p.

Therefore, in the pristine state this particular iron ore can be used as an electrocatalyst for both the HER and OER, where the latter reaction can be improved by mild electrochemical pre-treatment involving only 5 cycles of potential as shown in Figure S2. This activation process resulted in a morphology change at the surface as well the emergence of crystalline iron-nickel sulphide regions (Fe-and Ni_3S_2) and NiOOH (rather than a material dominated by iron sulphide such as Fe_7S_8). Clearly the reduction in the iron sulphide component resulted in a loss in the HER performance but the formation of NiOOH was beneficial for the OER. This conclusion was in accord with other studies which have shown that metal chalcogenides and more broadly selenides and phosphides were mostly precursors to the active form of the OER catalyst. However, the sulphide elements persisted as evidenced by the HRTEM and XPS data; thus indicating that they still played a role in the OER. As mentioned previously the formation of repulsive 3p–2p sites via the presence of electronegative sulphur atoms accelerated the oxidation of the –OOH intermediate formed during the OER.[18] In addition it has been well documented that the presence of Fe within a Ni hydroxide/oxyhydroxide network is beneficial for the OER.[49] Previous studies on amorphous NiFe(oxy)hydroxide mesoporous nanosheets deposited on nickel foam and a 2D Ni-Fe metal-organic framework also demonstrated the effectiveness of this combination; which showed excellent activity and stability.[50-51] For the system with Fe incorporated into $Ni(OH)_2$ the potential at which the $Ni(OH)_2$/NiOOH redox occurred prior to the OER, increased in the presence of Fe which also decreased the average oxidation state of Ni in NiOOH. It was this suppression of nickel into higher oxidation states which was responsible for excellent OER performance. In essence the OER activity of Ni cations is higher the lower the average oxidation state of Ni.[30] Therefore, in this investigation the formation of NiOOH at the surface in an Fe rich environment was attributed to the good OER performance of this ore.

Conclusion

The utilisation of naturally abundant materials as electrocatalysts for electrochemical water splitting has been demonstrated. The direct use of such a material without the need to chemically modify the bulk of the material through additional processing has the advantage and possibility of generating catalysts at a large scale that can otherwise be expensive using conventional industrial chemical synthesis processes. This particular mineral possesses the pyrrhotite and pentlandite phases which are the key components to its applicability as a HER and OER electrocatalyst. The presence of metal sulfide at the surface ensures HER activity while during the OER surface oxidation occurs to produce NiOOH which is the active species for this reaction. However the persistence of nickel sulphide at the surface was noted and also could influence the OER activity. Significantly, the active surface condition for the OER was achieved rapidly and required only mild electrochemical conditioning which remained stable for prolonged electrolysis. This study opens up an avenue of research to investigate many other minerals with suitable composition for not only this reaction but also that research could be directed to other materials synthesised in the Earth's crust that may appropriate chemical compositions suited to a vast array of chemical reactions.

Experimental Section

The raw iron ore material was obtained near Whitehorse, Yukon, Canada. The raw ore consisted of major species such as pyrrhotite and clinochlore with some sepolite, pentlandite, clinopyroxene, chalcopyrite, mica and galena. The raw material was crushed, ground, and sieved to remove 70 µm oversized particles. The microparticles were then directly used as electrode materials using Nafion 115® 117 (5 wt%) (Sigma Aldrich) as a binder. Sodium hydroxide (98%) (Sigma-Aldrich) 1 M solution was used as the electrolyte and made up with deionised water (resistivity of 18.2 MΩ cm) purified by use of a Milli-Q reagent deioniser (Millipore).

The catalyst suspension was prepared following the mass loading noted in the Table 1 with the addition of ethanol and Nafion® 117 (5 wt%, final concentration of 0.5 wt %) as the binder. The slurries were then sonicated for 30 min at room temperature. 20 µL of the catalyst ink was loaded on the glassy carbon rotary disk electrode (RDE) and dried at room temperature. Prior to dropcasting the sample, the working electrode surface was polished mechanically with 0.3 µm-sized alumina powder on a Microcloth pad and rinsed with Milli-Q water before sonication in ethanol for 2 minutes. The electrode surface was then rinsed with Milli-Q water several times. The deposited films were also washed with Milli-Q water several times ensuring no impurities remained on the surface.

Electrochemical characterisation of raw ore catalysts was undertaken at (20 ±2) ℃ with a BioLogic VSP workstation and a standard three-electrode

cell configuration, consisting of a working electrode, a reference electrode and a counter electrode. For RDE experiments a GC RDE (Rotary Disc Electrode) (2 mm diameter - Bioanalytical Systems) was used as the working electrode, and a platinum wire as an auxiliary electrode for the OER whereas a 1 mm diameter, Johnson Matthey Ultra "F" purity grade, carbon rod was used for the HER. The reference electrode was a Ag/AgCl (BASi) in all experiments.

For the OER the reproducibility of the measurements was achieved by carrying out three replicates for each experiment. In all cases iR correction was applied to all cyclic voltammograms and RDE experiments were carried out at 1500 rpm. For the OER data the potential was converted to the RHE scale via $E_{RHE} = E_{Ag/AgCl} + 0.059 \times pH + 0.197$ V where the activity of the hydroxide ions was considered at a concentration of one molar.[52] The current density reported in this work was normalised to the geometric surface area of the electrodes and was also used in the TOF calculation. The cyclic voltammetric experiments used to obtain the Tafel data were recorded at a sweep rate of 1 mV s^{-1}. All the electrochemical characterisation was completed in 1 M NaOH electrolyte solution.

X-ray photoelectron spectroscopy measurements were carried out using an AXIS Supra instrument (Kratos Analytical, UK) incorporating a monochromatic Al Kα X-ray source with a 15 mA emission current and total power of 225 W, which provided 300 × 700 µm area of interest. All the measurements were done using the charge neutraliser as a default, and samples were electrodeposited onto a GC substrate. Wide scans were recorded at an analyser pass energy of 160 eV with 0.5 eV steps and 300 ms dwell time. Narrow high-resolution scans for Ni 2p, Fe 2p, O 1s, S 2p and C 1s were taken at 20 eV pass energy, 0.2 eV steps, and 300 ms dwell time. The base pressure in the analysis chamber was 1.0×10^{-8} torr. One sweep was conducted for a wide scan whereas at least two sweeps were taken for narrow scans. Data analysis was done in CasaXPS licenced software following Shirley baseline with Kratos library Relative Sensitivity Factors (RSFs). Sample preparation for XPS measurements was the same as for SEM sample preparation. SEM and EDX were performed on a JEOL 7001F instrument at an operating voltage of 5 kV and 15 kV, respectively. HRTEM, SAED, STEM-DF, and STEM-EDX measurements were performed using a JEOL 2100 TEM instrument operating at an accelerating voltage of 200 kV. The JEOL 2100 machine was equipped with a high-sensitivity OXFORD 80 mm^2 silicon drift X-ray detector for accurate elemental analysis and JEOL BF/DF detectors for STEM imaging. The XRD patterns reported herein were recorded using either a Panalytical X'Pert MPD or Rigaku SmartLab XRD instrument. The Panalytical X'Pert instrument employed Cu-Kα radiation and used a gonio angle of 2.00° Omega.

Acknowledgements

AOM gratefully acknowledges the Australian Research Council for funding (DP180102869). The XPS, TEM, XRD and SEM data reported in this paper were obtained at the Central Analytical Research Facility operated by the Institute for Future Environments (IFE) at QUT. Access to CARF is supported by generous funding from the Science and Engineering Faculty, QUT

Keywords: Iron ore; water splitting; oxygen evolution; hydrogen evolution; electrocatalysis

[1] G. Glenk, S. Reichelstein, *Nat. Energy*. **2019**, *4*, 216-222.
[2] C. C. L. McCrory, S. Jung, I. M. Ferrer, S. M. Chatman, J. C. Peters, T. F. Jaramillo, *J. Am. Chem. Soc.* **2015**, *137*, 4347-4357.
[3] X. F. Lu, L. Yu, X. W. Lou, *Sci. Adv.* **2019**, *5*, eaav6009.
[4] Y. Shi, B. Zhang, *Chem. Soc. Rev.* **2016**, *45*, 1529-1541.
[5] A. I. Carim, F. H. Saadi, M. P. Soriaga, N. S. Lewis, *J. Mater. Chem. A*. **2014**, *2*, 13835-13839.
[6] W. Zhang, Y. Wu, J. Qi, M. Chen, R. Cao, *Adv. Energy Mater.* **2017**, *7*, 1602547.
[7] H. Liang, A. N. Gandi, C. Xia, M. N. Hedhili, D. H. Anjum, U. Schwingenschlögl, H. N. Alshareef, *ACS Energy Lett.* **2017**, *2*, 1035-1042.
[8] Y. Li, C. Zhao, *ACS Catal.* **2017**, *7*, 2535-2541.
[9] S. Zou, M. S. Burke, M. G. Kast, J. Fan, N. Danilovic, S. W. Boettcher, *Chem. Mater.* **2015**, *27*, 8011-8020.
[10] X. Zhou, Z. Xia, Z. Tian, Y. Ma, Y. Qu, *J. Mater. Chem. A*. **2015**, *3*, 8107-8114.
[11] S. Dresp, F. Luo, R. Schmack, S. Kuhl, M. Gliech, P. Strasser, *Energy Environ. Sci.* **2016**, *9*, 2020-2024.
[12] U. K. Sultana, J. D. Riches, A. P. O'Mullane, *Adv. Funct. Mater*. **2018**, *28*, 1804361.
[13] M. Browne, R. J. Cullen, R. L. Doyle, P. E. Colavita, M. E. G. Lyons, *ECS Trans.* **2013**, *53*, 59-77.
[14] Y.-F. Li, Z.-P. Liu, *J. Am. Chem. Soc.* **2018**, *140*, 1783-1792.
[15] U. K. Sultana, A. P. O'Mullane, *ACS Appl. Energy Mater.* **2018**, *1*, 2849-2858.
[16] M. A. R. Anjum, J. S. Lee, *ACS Catal.*,**2017**, *7*, 3030-3038.
[17] J. Kibsgaard, T. F. Jaramillo, *Angew. Chem. Int. Ed.* **2014**, *53*, 14433-14437.
[18] J. Joo, T. Kim, J. Lee, S.-I. Choi, K. Lee, *Adv. Mater.* **2019**, *31*, 1806682.
[19] N. Xue, P. Diao, *J. Phys. Chem. C*. **2017**, *121*, 14413-14425.
[20] I. Roger, M. A. Shipman, M. D. Symes, *Nat. Rev. Chem.* **2017**, *1*, 0003.
[21] X. Zou, Y. Zhang, *Chem. Soc. Rev.* **2015**, *44*, 5148-5180.
[22] P. Du, R. Eisenberg, *Energy Environ. Sci.* **2012**, *5*, 6012-6021.
[23] I. Godwin, A. Rovetta, M. Lyons, J. Coleman, *Curr. Opinion Electrochem.* **2018**, *7*, 31-35.
[24] S. Jin, *ACS Energy Lett.* **2017**, *2*, 1937-1938.
[25] U. K. Sultana, A. P. O'Mullane, *ChemElectroChem*. **2019**, *6*, 2630-2637.
[26] Y. Uchino, T. Kobayashi, S. Hasegawa, I. Nagashima, Y. Sunada, A. Manabe, Y. Nishiki, S. Mitsushima, *Electrocatal.* **2018**, *9*, 67-74.
[27] B. Konkena, K. junge Puring, I. Sinev, S. Piontek, O. Khavryuchenko, J. P. Dürholt, R. Schmid, H. Tüysüz, M. Muhler, W. Schuhmann, U.-P. Apfel, *Nat. Commun.* **2016**, *7*, 12269.
[28] F. Le Formal, N. Guijarro, W. S. Bouree, A. Gopakumar, M. S. Prevot, A. Daubry, L. Lombardo, C. Sornay, J. Voit, A. Magrez, P. J. Dyson, K. Sivula, *Energy Environ. Sci.* **2016**, *9*, 3448-3455.
[29] M. A. Sayeed, J. F. S. Fernando, A. P. O'Mullane, *Adv. Sust. Systems*. **2018**, *2*, 1800019.
[30] M. W. Louie, A. T. Bell, *J. Am. Chem. Soc.* **2013**, *135*, 12329-12337.
[31] M. Görlin, P. Chernev, J. Ferreira de Araújo, T. Reier, S. Dresp, B. Paul, R. Krähnert, H. Dau, P. Strasser, *J. Am. Chem. Soc.* **2016**, *138*, 5603-5614.
[32] M. A. Sayeed, A. P. O'Mullane, *RSC Adv.* **2017**, *7*, 43083-43089.
[33] N. Jiang, Q. Tang, M. Sheng, B. You, D.-e. Jiang, Y. Sun, *Catal. Sci. Technol.* **2016**, *6*, 1077-1084.
[34] R. Miao, B. Dutta, S. Sahoo, J. He, W. Zhong, S. A. Cetegen, T. Jiang, S. P. Alpay, S. L. Suib, *J. Am. Chem. Soc.* **2017**, *139*, 13604-13607.
[35] L. Pei, Y. Yang, H. Chu, J. Shen, M. Ye, *Ceramics Internat.* **2016**, *42*, 5053-5061.
[36] S. Chen, Z. Kang, X. Zhang, J. Xie, H. Wang, W. Shao, X. Zheng, W. Yan, B. Pan, Y. Xie, *ACS Central Sci.* **2017**, *3*, 1221-1227.
[37] J. Yu, G. Cheng, W. Luo, *J. Mater. Chem. A*. **2017**, *5*, 15838-15844.
[38] C.-Z. Yuan, Z.-T. Sun, Y.-F. Jiang, Z.-K. Yang, N. Jiang, Z.-W. Zhao, U. Y. Qazi, W.-H. Zhang, A.-W. Xu, *Small* **2017**, *13*, 1604161.
[39] T. Pandiarajan, L. John Berchmans, S. Ravichandran, *RSC Adv.* **2015**, *5*, 34100-34108.

[40] M. Manolova, C. Schoeberl, R. Freudenberger, C. Ellwein, J. Kerres, S. Stypka, B. Oberschachtsiek, *Int. J. Hydrogen Energy* **2015**, *40*, 11362-11369.
[41] A. de Aldecoa, F. Roldán, C. Menor-Salván, *Life* **2013**, *3*, 502.
[42] M. Pósfai, G. Sharp Thomas, A. Kontny, in *American Mineralogist*, 2000, p. 1406.
[43] N. Zhang, W. Q. Han, L. J. Wang, *Adv. Mater. Res.* **2012**, *356-360*, 1367-1370.
[44] P. Ganesan, A. Sivanantham, S. Shanmugam, *J. Mater. Chem. A*. **2016**, *4*, 16394-16402.
[45] Y. Yang, Q. Tao, G. Srinivasan, C. G. Takoudis, *J. Solid State Sci. Technol*. **2014**, *3*, P345-P352.
[46] D. L. Legrand, G. M. Bancroft, H. W. Nesbitt, *American Mineralogist*, **2005**, *90*, 1042-1054.
[47] V. Krylova, M. Andrulevicius, *Int. J. Photoenergy*. **2009**, *2009*, 304308.
[48] J.-Q. Chi, X. Shang, S.-S. Lu, B. Dong, Z.-Z. Liu, K.-L. Yan, W.-K. Gao, Y.-M. Chai, C.-G. Liu, *Carbon*. **2017**, *124*, 555-564.
[49] L. Trotochaud, S. L. Young, J. K. Ranney, S. W. Boettcher, *J. Am. Chem. Soc.* **2014**, *136*, 6744-6753.
[50] C. Xiao, Y. Li, X. Lu, C. Zhao, *Adv. Funct. Mater.* **2016**, *26*, 3515-3523.
[51] J. Duan, S. Chen, C. Zhao, *Nat. Commun.* **2017**, *8*, 15341.
[52] S. Licht, *Anal. Chem.* **1985**, *57*, 514-519.